Low-temperature linear thermal rectifiers based on Coriolis forces

Suwun Suwunnarat, Huanan Li, Ragnar Fleischmann, and Tsampikos Kottos

Phys. Rev. E **93**, 042115 — Published 14 April 2016

DOI: 10.1103/PhysRevE.93.042115

Low-Temperature Linear Thermal Rectifiers Based on Coriolis forces

Suwun Suwunnarat[1], Huanan Li[1], Ragnar Fleischmann[2] and Tsampikos Kottos[1,2]
[1]*Department of Physics, Wesleyan University, Middletown, Connecticut 06459, USA*
[2]*Max Planck Institute for Dynamics and Self-organization (MPIDS), 37077 Göttingen, Germany*

We demonstrate that a three-terminal harmonic symmetric chain in the presence of a Coriolis force, produced by a rotating platform which is used to place the chain, can produce thermal rectification. The direction of heat flow is reconfigurable and controlled by the angular velocity Ω of the rotating platform. A simple three terminal triangular lattice is used to demonstrate the proposed principle.

PACS numbers: 44.10.+i, 05.60.-k, 66.70.-f

I. INTRODUCTION

In the last few years considerable research effort has been invested in developing appropriately engineered structures that display novel transport properties not found in nature. In the thermal transport framework, this activity has recently started to gain a lot of attention. Apart from the purely academic reasons, there is a growing consensus on its practical implications in the efforts of the society to manage its energy resources efficiently. Thus research programs that aim to propose new methods, designs or materials that allow to harness and mold the heat flow at the nanoscale level in ways that can affect society's energy consumption needs are at the forefront of the research agenda. Some of the targets that are within our current nanotechnology capabilities include the generation of nanoscale heat-voltage converters, thermal transistors and rectifiers, nanoscale radiation detectors, heat pumps and even thermal logic gates [1–6].

In spite of these efforts the understanding of thermal transport and more importantly the manipulation of heat current is still in its infancy. This becomes more obvious if one compares with the tremendous achievements of the last fifty years in understanding and managing electron transport. In contrast, for example, the important problem of thermal rectification is addressed only by a handful of researchers. For example, the investigation of radiative thermal rectification, both in the nearfield and farfield regimes, has recently attracted attention [7–9]. In the case of phononic heat transport, the majority of the existing proposals rely on the interplay of system non-linearities with structural asymmetries [10–12]. At the nanoscale limit where the phonon mean-free path is comparable to the size of the devices the inherent nonlinearities are irrelevant and transport is fully dominated by ballistic phonon transport (ballistic limit). However recently it was shown in Ref. [13–15] that in the ballistic regime one can achieve thermal rectification under very specific conditions: low temperature limit associated with quantum harmonic systems in the nonlinear response domain, and the presence of a third reservoir which acts as a probe and it is coupled asymmetrically with the rest of the system in order to break any spatial symmetry. The importance of asymmetry of the system itself was further highlighted in Ref. [15].

In this paper we focus on the development of a new concept for the creation of unidirectional thermal valves that control and direct heat currents on the nanoscale level. Specifically we propose to create a ballistic symmetric thermal rectifier which relies on Coriolis forces. In contrast to previous studies our proposal does not rely on any structural asymmetry. Rather, an asymmetry is induced in a very controllable way by the Coriolis force allowing a high flexibility in the rectification properties without a change of the structural setup. The system consists of a symmetric harmonic lattice placed on a rotating platform with angular velocity Ω. The direction of heat current is controlled on the sign of Ω, thus allowing for a reconfigurable heat current management. A schematic of such set-up, consisting of three harmonic masses coupled to a rotating platform, is shown in Fig. 1. Using the non-equilibrium Green's function formalism we derive the conditions of optimal operation of the structure. Subsequently we have verified these predictions via detailed numerical calculations using a simple variant of the proposed structure.

The paper is organized as follows. In section II we present the theoretical model. The mathematical formalism for the evaluation of heat current and the conditions for non-reciprocity are discussed in section III. Finally a numerical confirmation of our predictions are given in section IV. Our conclusions are given in the last section V.

II. THEORETICAL MODEL

We consider a harmonic lattice of N particles coupled together with spring constants k^C. All particles are assumed to have the same mass m. Below, without any loss of generality, we assume that all masses are $m = 1$. The lattice is placed on a platform in the $X - Y$ plane. Thus each particle can move on this platform and has $D = 2$ degrees of freedom. The connectivity of the lattice is

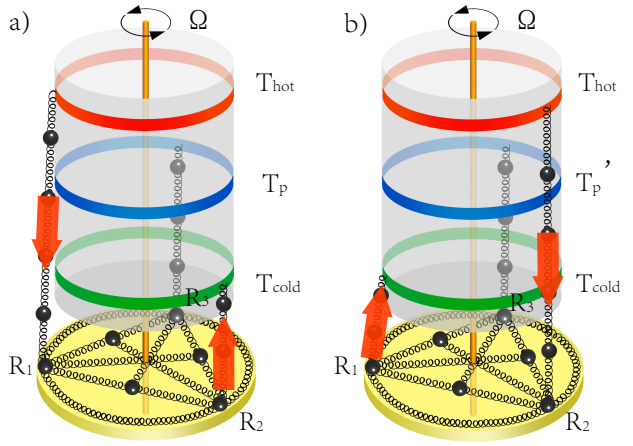

FIG. 1: (Color on-line) A schematic of the thermal rectifier due to rotation when $N_b = 1$: on each edge of the triangle, masses are coupled together with equal harmonic springs up to the next-nearest neighbor. The masses are also attached to a post with similar springs and they move on a platform (substrate) at the $X-Y$ plane which rotates with a counterclockwise (CCW) angular velocity Ω. Additionally these masses are coupled to the substrate with springs that have coupling constants k_0 (not shown in the figure). a) The mass R_1 is coupled to a high-temperature bath with temperature $T_{R_1} = T_{hot}$ while the mass R_2 is coupled to the low-temperature bath with temperature $T_{R_2} = T_{cold}$. The mass R_3 is connected to the probe bath with temperature $T_{R_3} = T_p$. b) The mass R_1 is coupled to a low-temperature bath with temperature $T_{R_1} = T_{cold}$ while the mass R_2 is coupled to the high-temperature bath with temperature $T_{R_2} = T_{hot}$. The mass R_3 is again connected to the probe bath with a different temperature $T_{R_3} = T_p'$.

uniquely defined by the $\mathcal{N} = N * D$ dimensional symmetric force matrix K^C. We will assume the most general case where the coupling is not necessarily confined to be only between nearest (in space) masses. Moreover we will assume that all masses are coupled harmonically to a central post which is parallel to the Z axis and placed in the middle of the platform.

The lattice rotates around the post with a constant angular velocity $\overrightarrow{\Omega}$. It is useful to describe the motion of the system in the rotating frame. In this frame the particles are characterized by their equilibrium position vector $R^0 = (R_1^0, \cdots, R_N^0)^T$, by their displacements vector $S = (S_1^x, S_1^y, S_1^z, \cdots, S_N^x, S_N^y, S_N^z)^T$ and the associated conjugate canonical momenta vector $p_C = (p_{C1}^x, p_{C1}^y, p_{C1}^z, \cdots, p_{CN}^x, p_{CN}^y, p_{CN}^z)^T$ (the superscript T indicates transposition). The Hamiltonian that describes the system in the rotating frame takes the form:

$$H_C = \frac{1}{2} p_C^T p_C + \frac{1}{2} S^T K^C S - \left(R^0 + S\right)^T A\, p_C \qquad (1)$$

where A is the $\mathcal{N} \times \mathcal{N}$ block-diagonal matrix

$$A = \mathrm{diag}\{\tilde{A}_D\}; \tilde{A}_{D=3} = \begin{bmatrix} \tilde{A}_{D=2} & 0 \\ 0 & 0 \end{bmatrix}; \tilde{A}_{D=2} = \begin{bmatrix} 0 & \Omega \\ -\Omega & 0 \end{bmatrix} \qquad (2)$$

with the property $A^T = -A$. The last term in Eq. (1) describes the Coriolis force in the rotating frame.

The rotating lattice described by Eq.(1) is coupled with three equivalent co-rotating heat baths. The latter are always attached to the same three particles of the lattice $\alpha = R_1, R_2, R_3$. We will assume that two of these baths are at high T_{hot} and low T_{cold} constant temperatures, respectively. The third bath acts as a probe and its temperature $T_{R_3} = T_p$ is adjusted self-consistently such that the net heat flux from it is zero. In general this can lead to different T_p values in the forward ($T_{R_1} = T_{\mathrm{hot}}$ and $T_{R_2} = T_{\mathrm{cold}}$) and backward ($T_{R_1} = T_{\mathrm{cold}}$ and $T_{R_2} = T_{\mathrm{hot}}$) process.

For simplicity, the heat baths are described quasi-classically, i.e. we promote the relative momenta p_α of the $\alpha-$bath particles and their displacements u_α, with respect to the rotating frame, to conjugate canonical pairs [16]. Nevertheless, we assume that the statistical properties of the phonons in these thermal reservoirs are not affected by the Coriolis force and respect quantum statistics [14]. The three baths, each consisting of an infinite number of harmonically coupled bath particles, are described by Hamiltonians

$$H_\alpha = \frac{1}{2} p_\alpha^T p_\alpha + \frac{1}{2} u_\alpha^T K^\alpha u_\alpha,\ \alpha = R_1, R_2, R_3 \qquad (3)$$

with a (semi-infinite) harmonic force matrix $K^\alpha = (K^\alpha)^T$ contains additional $-\left|\overrightarrow{\Omega}\right|^2 \cdot I$ terms due to the centrifugal force (I denotes the semi-infinite identity matrix).

Finally we have assumed that each particle is pinned to the substrate (i.e. the rotating platform, see Fig. 1 for a special case of three masses) via a quadratic potential with a coupling constant k_0. This pinning potential guarantees that the lattice particles have an equilibrium position and it can be incorporated easily in all force matrices K^C, K^α, see Eqs. (1) and (3).

We are now ready to write down the total Hamiltonian of the bath-lattice system which takes the form:

$$H_{tot} = H_C + \sum_\alpha H_\alpha + \sum_\alpha H_{\alpha C} \qquad (4)$$

where $H_{\alpha C} = u_\alpha^T V^{\alpha C} u_C$ describes the coupling between the lattice particles and the heat baths.

Below we will be assuming that the initial condition of the total system is a direct product state

$$\hat{\rho}_{ini}\left(t_0\right) = \prod_\alpha \otimes \frac{e^{-H_\alpha/(k_B T_\alpha)}}{\mathrm{Tr}\left(e^{-H_\alpha/(k_B T_\alpha)}\right)} \otimes \frac{e^{-H_C/(k_B T_C)}}{\mathrm{Tr}\left(e^{-H_C/(k_B T_C)}\right)} \qquad (5)$$

which after sufficient long time will be relaxing to a steady state $\hat{\rho}^{ss}$. Note that the temperature of the two

baths T_α are kept constant and the steady-state thermal current will not depend on the initial temperature of the lattice model T_C. The value of the temperature of the probe in the non-equilibrium steady state (NESS) will be determined by the temperature of the other baths.

III. FORMALISM

A. Heat Current

We want to calculate the steady-state thermal current flowing from the hot reservoir $T_{\rm hot}$ towards the cold reservoir $T_{\rm cold}$. To this end we will employ the standard non-equilibrium Green's function technique [18–20]. The steady-state current out of the heat bath α is

$$\begin{aligned} I_\alpha &\equiv -\mathrm{Tr}\left[\hat{\rho}^{ss}\frac{d\hat{H}_\alpha(t)}{dt}\right] \\ &= \sum_{\gamma\neq\alpha}\int_0^\infty \frac{d\omega}{2\pi}\hbar\omega\mathcal{T}_{\gamma\alpha}[\omega](f_\alpha - f_\gamma). \end{aligned} \tag{6}$$

where $f_\alpha = f(\omega,T_\alpha) = \{\exp(\hbar\omega/k_BT_\alpha)-1\}^{-1}$ is the Bose distribution associated with the particles at the bath α which have fixed temperature T_α and $\mathcal{T}_{\gamma\alpha}$ is the transmission coefficient from the α-th bath to the γ-th bath. The hot and cold reservoirs, with temperatures $T_{\rm hot}$ and $T_{\rm cold}$, will be attached to the particles R_1, R_2 while the third - probe - reservoir with varying temperature T_p will be always attached to the R_3-particle.

During the forward process we attach the hot reservoir to the particle R_1 so that $T_{R_1} = T_{\rm hot}$ and the cold reservoir, to the particle R_2 so that $T_{R_2} = T_{\rm cold}$. The associated heat current I_f out of bath R_2 is then given from Eq. (6)

$$I_f = \sum_{\gamma=R_1,R_3}\int_0^\infty \frac{d\omega}{2\pi}\hbar\omega\mathcal{T}_{\gamma,R_2}[\omega](f(T_{R_2}) - f(T_\gamma)). \tag{7}$$

where a negative value in I_f will indicate current flowing from the hot reservoir to the cold reservoir. The bath temperature $T_{R_3} = T_p^f$ associated with the probe reservoir has to be evaluated from the requirement that the net current I_p flowing in the probe reservoir is zero i.e.

$$I_p = \sum_{\gamma=R_1,R_2}\int_0^\infty \frac{d\omega}{2\pi}\hbar\omega\mathcal{T}_{\gamma,R_3}[\omega]\left(f(T_p^f) - f(T_\gamma)\right) = 0. \tag{8}$$

The backward process is associated with the reverse configuration i.e. $T_{R_2} = T_{\rm hot}$ and $T_{R_1} = T_{\rm cold}$. The associated heat flux I_b out of bath R_2 and the corresponding temperature of the probe T_p^b are derived using similar relations as the ones shown in Eqs. (7,8).

For the probe temperatures in the forward and backwards process, respectively, we find:

$$\begin{aligned} T_p^f &= T_0 + a\Delta T + g\Delta T^2 + O(\Delta T^3) \\ T_p^b &= T_0 - a\Delta T + g\Delta T^2 + O(\Delta T^3) \end{aligned} \tag{9}$$

where $T_{\rm hot/cold} = T_0 \pm \Delta T$. The constants a, g are

$$\begin{aligned} a &= -\frac{\int_0^\infty \frac{d\omega}{2\pi}\hbar\omega(\mathcal{T}_{R_2,R_3} - \mathcal{T}_{R_1,R_3})\frac{\partial f}{\partial T}|_{T_0}}{\int_0^\infty \frac{d\omega}{2\pi}\hbar\omega(\mathcal{T}_{R_2,R_3} + \mathcal{T}_{R_1,R_3})\frac{\partial f}{\partial T}|_{T_0}} \\ g &= \frac{(1-a^2)}{2}\frac{\int_0^\infty \frac{d\omega}{2\pi}\hbar\omega(\mathcal{T}_{R_2,R_3} + \mathcal{T}_{R_1,R_3})\frac{\partial^2 f}{\partial T^2}|_{T_0}}{\int_0^\infty \frac{d\omega}{2\pi}\hbar\omega(\mathcal{T}_{R_2,R_3} + \mathcal{T}_{R_1,R_3})\frac{\partial f}{\partial T}|_{T_0}}. \end{aligned} \tag{10}$$

B. The Transmission Coefficient

We proceed with the evaluation of the transmission coefficient $\mathcal{T}_{\gamma\alpha}$. The latter is needed for the calculation of the forward and backward currents, and therefore for the evaluation of the rectification parameter R via Eq. (17). The transmission coefficients can be expressed as

$$\mathcal{T}_{\gamma\alpha}[\omega] = \mathrm{Tr}\left[G^r_{CC}\Gamma_\gamma G^a_{CC}\Gamma_\alpha\right]; \quad \Gamma_\alpha \equiv i\left[\Sigma^r_\alpha - \Sigma^a_\alpha\right] \tag{11}$$

where $G^{r(a)}_{CC}$ is the the retarded (advanced) Green's functions of the lattice. $\Sigma^{r(a)}_\alpha = \left(V^{\alpha C}\right)^T g^{r(a)}_\alpha V^{\alpha C}$ is the associated self-energy which can be expressed in terms of the equilibrium Green's function $g^{r(a)}_\alpha$ of the isolated heat bath α and the coupling matrix $V^{\alpha C}$. Moreover using the definition Eq. (11) we can deduce that Γ_α is a symmetric matrix i.e $\Gamma^T_\alpha = \Gamma_\alpha$.

The retarded Green's function G^r_{CC} for the central junction in the frequency domain takes the form

$$G^r_{CC}[\omega] = \left[\left(\omega + i0^+\right)^2 - K^C - \Sigma^r[\omega] - A^2 - 2i\omega A\right]^{-1} \tag{12}$$

where $\Sigma^r = \sum_\alpha \Sigma^r_\alpha$ denotes the total retarded self-energy due to the interaction with all the heat baths. The associated advanced Green function can be expressed in terms of G^r_{CC} as

$$G^a_{CC}[\omega] = \left(G^r_{CC}[\omega]\right)^\dagger. \tag{13}$$

Using expression Eq. (12) we can deduce that

$$G^{r(a)}_{CC}[\omega,-\Omega] = G^{r(a)}_{CC}[\omega,\Omega]^T. \tag{14}$$

Using the cyclic property of the trace, the symmetric nature of further $\Gamma^T_\alpha = \Gamma_\alpha$ and Eq. (14), we can easily show that

$$\mathcal{T}_{\gamma\alpha}[\omega,-\Omega] = \mathcal{T}_{\alpha\gamma}[\omega,\Omega] \neq \mathcal{T}_{\gamma\alpha}[\omega,\Omega] \tag{15}$$

which lead us to the conclusion that for $\Omega \neq 0$ the time-reversal symmetry of the system is broken due to the rotation.

In order to highlight the importance of the Coriolis force in thermal rectification we will be considering setups which involve structural rotational symmetry. In this case, any asymmetric heat transport phenomena that we will find are due to Coriolis force only (contrast this with the studies of Refs. [10–12] where thermal rectification is due to structural asymmetries). As an outcome of this

rotational symmetry assumption we have that the transmission coefficients $\mathcal{T}_{\alpha,\gamma}$ satisfy the following relations

$$\mathcal{T}_{R_2R_1} = \mathcal{T}_{R_3R_2} = \mathcal{T}_{R_1R_3},\ \mathcal{T}_{R_1R_2} = \mathcal{T}_{R_2R_3} = \mathcal{T}_{R_3R_1}. \quad (16)$$

The above expressions can allow us to calculate the transmission coefficient $\mathcal{T}_{\gamma\alpha}[\omega]$, and thus to proceed with the evaluation of the forward and backward currents I_f, I_b.

C. The Rectification Parameter

Below we will quantify the rectification effect by the rectification parameter R defined as

$$R = \frac{-\Delta I}{\max\{|I_f|, |I_b|\}}; \quad \Delta I = I_f + I_b. \quad (17)$$

When $\Delta I > 0$ ($R < 0$) the system acts as a thermal rectifier favoring the direction from the bath placed at R_2 to the bath attached at R_1 while the reverse is true in case that $\Delta I < 0$ ($R > 0$). We will assume $T_{\rm hot/cold} = T_0 \pm \Delta T$ and analyze the dependence of R on the temperature difference ΔT.

Using Eqs. (6,8,16) we can evaluate the rectification parameter R up to the second order in the temperature difference ΔT. The current difference ΔI is given by [14]:

$$\Delta I = (1-a^2)\frac{K}{F(\mathcal{T}_{R_2R_3}) + F(\mathcal{T}_{R_1R_3})}\Delta T^2 \quad (18)$$

where the parameter a has been already defined in Eq. (10) and its absolute value is always smaller than unity i.e. $|a| \leq 1$. Therefore the coefficient $(1-a^2)$ appearing in Eq. (18) is always greater than zero i.e. $(1-a^2) > 0$. The positive definite functions $F(\mathcal{T}_{\alpha R_3}) > 0$ are defined as $F(\mathcal{T}_{\alpha R_3}) = \int_0^\infty \frac{d\omega}{2\pi}\hbar\omega\left(\frac{\partial f(\omega,T)}{\partial T}\right)_{T_0}\mathcal{T}_{\alpha R_3}$, $\alpha = R_1, R_2$. Finally K in Eq. (18) is defined as

$$K = \int_0^\infty \frac{d\omega_1}{2\pi}\int_{\omega_1}^\infty \frac{d\omega_2}{2\pi} W(\omega_1,\omega_2,T_0)\mathcal{T}(\omega_1,\omega_2); \quad (19)$$
$$W = \frac{\hbar^3\omega_1\omega_2}{k_B T_0^2}\left(\frac{\partial f(\omega_1,T)}{\partial T}\frac{\partial f(\omega_2,T)}{\partial T}\right)_{T_0}\{\omega_2(1+2f(\omega_2,T_0)) - \omega_1(1+2f(\omega_1,T_0))\}$$

with the weight function W and $\mathcal{T}(\omega_1,\omega_2) = \mathcal{T}_{R_2R_3}[\omega_1]\mathcal{T}_{R_2R_3}[\omega_2]\left\{\frac{\mathcal{T}_{R_1R_3}[\omega_2]}{\mathcal{T}_{R_2R_3}[\omega_2]} - \frac{\mathcal{T}_{R_1R_3}[\omega_1]}{\mathcal{T}_{R_2R_3}[\omega_1]}\right\}$.

From Eq. (18) and the subsequent discussion we can draw a number of conclusions: Since the linear term in the ΔT expansion is zero we immediately conclude that in the linear-response regime or in the classical limit our system has zero rectification parameter, i.e. $R = 0$,and therefore one needs to consider the quantum regime beyond linear response. Second, we realize that since $1 - a^2 > 0$ and $F(\mathcal{T}_{\alpha R_3}) > 0$, the sign of ΔI (and thus the sign of the rectification parameter R) is completely determined by the sign of K, see Eq. (19). Below we will be confirming these predictions for a simplified version of our model Eq. (4).

IV. AN EXAMPLE OF THERMAL RECTIFICATION DUE TO CORIOLIS FORCE

We will demonstrate the rectification effect, induced by the Coriolis force ($\Omega \neq 0$), using a simple version of the general model, Eq. (4). The underlying *symmetric* harmonic lattice has an equilibrium configuration associated with an equilateral triangle. Each of the three corners of the triangle R_1^0, R_2^0, R_3^0 are occupied by equal masses R_1, R_2, R_3, coupled with the same harmonic coupling k_C to a post which is placed at the center O of the triangle. On every edge of the triangle, say for example edge $R_1^0R_2^0$, (by excluding the masses at the vertexes) there are additional N_b equal masses, which are connected with the center O of the triangle by springs dividing the angle $\angle R_1^0 O R_2^0$ equally. An equal harmonic coupling up to the next-nearest neighbor is considered between the masses on each edge of the triangle. Furthermore, the masses R_1, R_2, R_3 are attached to three equivalent 1D Rubin baths [21]. The 1D Rubin baths $\alpha = R_1, R_2, R_3$ are made up of a semi-infinite spring chain with $K^\alpha_{nm} = \delta_{nm}(2k^\alpha - \Omega^2 + k_0) - k^\alpha\delta_{n\pm1,m}$. Here an additional coupling k_0 with the substrate is assumed. An illustration of our model with $N_b = 1$ is shown in Fig. 1.

The symmetric force matrix K^C in Eq. (1) can be obtained systematically as follows. Each spring (harmonic coupling) will contribute to the matrix K^C with an additive harmonic term. These spring contributions can be classified in three categories. First, we consider the coupling between two masses R_j and R_k of the system. We use local Euclidean coordinate system to describe the relative displacement of the particles with respect to their equilibrium positions. The local Euclidean coordinate system for each particle is specified in the following way: its origin is taken as the equilibrium position of the particle and its x-axis and y-axis respectively coincide with the radial (r) and tangential direction (θ) of fixed equilib-

rium position of the specific particle. Specifically, using this local Euclidean coordinate system, the contribution of the spring connecting the particles R_j, R_k to the matrix K^C is

$$\begin{aligned}
[K^C]_{jr_j,jr_j} &= [K^C]_{j\theta_j,j\theta_j} = [K^C]_{kr_k,kr_k} = [K^C]_{k\theta_k,k\theta_k} = k_C \\
[K^C]_{jr_j,kr_k} &= [K^C]_{kr_k,jr_j} = -k_C \cos(\theta_j^0 - \theta_k^0) \\
[K^C]_{jr_j,k\theta_k} &= [K^C]_{k\theta_k,jr_j} = -k_C \sin(\theta_j^0 - \theta_k^0) \\
[K^C]_{j\theta_j,kr_k} &= [K^C]_{kr_k,j\theta_j} = k_C \sin(\theta_j^0 - \theta_k^0) \\
[K^C]_{j\theta_j,k\theta_k} &= [K^C]_{k\theta_k,j\theta_j} = -k_C \cos(\theta_j^0 - \theta_k^0). \qquad (20)
\end{aligned}$$

where $\left(r_j^0, \theta_j^0\right)$ and $\left(r_k^0, \theta_k^0\right)$ is the polar coordinate for the equilibrium positions R_j^0 and R_k^0 of two masses R_j and R_k. Second, we evaluate the contribution to the matrix K^C due to the spring coupling between the mass R_j and the center O. We have that $[K^C]_{jr_j,jr_j} = [K^C]_{j\theta_j,j\theta_j} = k_C$. Similarly the coupling between the mass R_j and the platform provides the contribution $[K^C]_{jr_j,jr_j} = [K^C]_{j\theta_j,j\theta_j} = k_0$. Third, due to the coupling with the bath α additional terms are added to the matrix K^C. For example, for $\alpha = R_1$ they are $[K^C]_{1r_1,1r_1} = [K^C]_{1\theta_1,1\theta_1} = k^{R_1}$.

Finally the nonzero elements of the coupling matrices (see below Eq. (4) for a definition) are respectively $\left[V^{R_1C}\right]_{1,1r_1} = -k^{R_1}$, $\left[V^{R_2C}\right]_{1,2r_2} = -k^{R_2}$ and $\left[V^{R_3C}\right]_{1,3r_3} = -k^{R_3}$. In the following, $k^{R_1} = k^{R_2} = k^{R_3} = k$ is assumed for simplicity.

The thermal rectification effect is present when the (structurally) symmetric system is rotating with an angular velocity Ω around the post situated at the center O. To be specific, first the bath coupled to the mass R_1 is set to the higher temperature $T_{R_1} = T_{hot} = T_0 + \Delta T$ and the bath coupled to the mass R_2 is set to the lower temperature $T_{R_2} = T_{cold} = T_0 - \Delta T$ (forward process). The temperature T_p of the probe bath coupled to the mass R_3 is determined by the zero flux condition as discussed above. We then calculate the forward thermal current I_f using Eq. (7). Second, by reversing the temperature bias, *i.e.*, $T_{R_2} = T_{hot}$ and $T_{R_1} = T_{cold}$, and adjusting the temperature of the probe bath R_3 to be T_p', the thermal current I_b for the backward process is evaluated. In the following natural units are assumed, i.e. $\hbar = 1$, $m = 1$, $k = 1$, $k_B = 1$.

Our numerical results for the rectification parameter R versus the angular velocity Ω and different average temperatures T_0 are shown in Fig. 2a. These data clearly demonstrate that the rectification effect is present once $\Omega \neq 0$. Figure 2a confirms that for high average temperatures T_0, corresponding to the classical limit, the rectification effect is suppressed (compare e.g. the curves for $T_0 = 0.1$ and $T_0 = 3$) as we have predicted in subsection III C.

From Fig. 2a we further see that the rectification parameter R for a fixed angular velocity may change sign when the average temperature T_0 changes from 0.1 to 0.4. This can be understood from the perturbation result in Eq. (18). Figure 3 demonstrates that, when the average temperature T_0 changes from 0.1 to 0.4, the frequency region for which the absolute value of the weight function $|W(\omega_1, \omega_2, T_0)|$ is large will shifts towards high frequencies. Bearing this fact in mind, we are now able to explain the change of sign in the rectification. For example, for $\Omega = 0.03$, we find that the transmission ra-

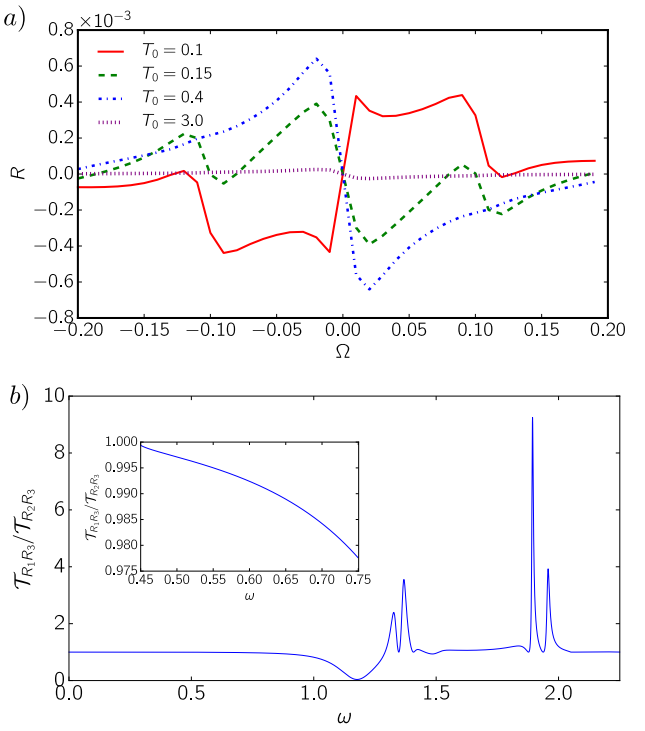

FIG. 2: (Color on-line) a) Plots of rectification R versus angular velocity Ω for different average temperatures T_0. b) A plot of the transmission coefficient ratio $\frac{\mathcal{T}_{R_1R_3}}{\mathcal{T}_{R_2R_3}}$ versus frequency ω, with the fixed angular velocity $\Omega = 0.03$. The inset shows this ratio from $\omega = 0.45$ to 0.75. Other parameters are $N_b = 4$, $k_C = k = 1$ and $\Delta T = 2.5\%T_0$.

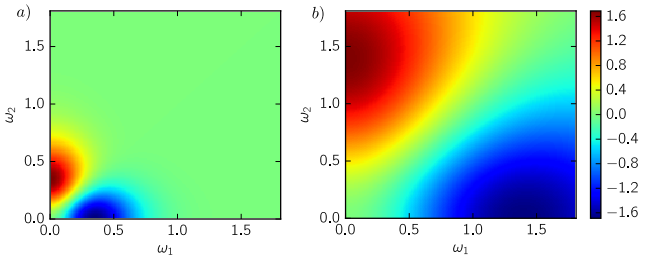

FIG. 3: (Color on-line) A density plot of the weight function $W(\omega_1, \omega_2, T_0)$ versus ω_1 and ω_2 for two different average temperatures a) $T_0 = 0.1$ and b)$T_0 = 0.4$. Clearly, when the average temperature T_0 increases, the dominant part of the magnitude of the weight-function $|W(\omega_1, \omega_2, T_0)|$ moves to the higher frequency.

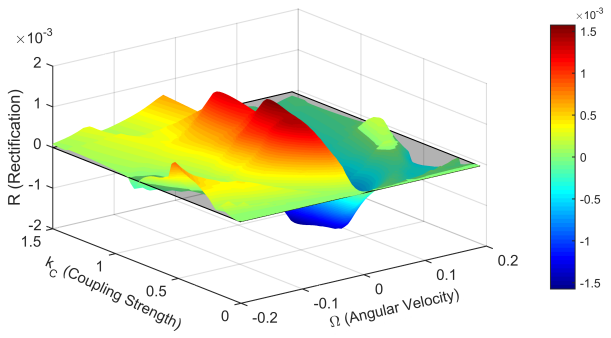

FIG. 4: (Color on-line) A 3D plot of rectification R versus angular velocity Ω and spring constant k_C in the center lattice. Other parameter are $N_b = 4$, $T_0 = 0.4$, $k = 1$ and $\Delta T = 2.5\%T_0$. At $k_c \approx 0.65$ and $\Omega \approx \pm 0.02$ the rectification gets its maximum value.

tio $\frac{\mathcal{T}_{R_1R_3}}{\mathcal{T}_{R_2R_3}}$ initially decreases as a function of frequency while for larger frequencies it increases, see Fig. 2 b). As a result K (see Eq. (19)) changes sign from negative to positive so that the rectification parameter R Eq. (18) changes also sign from positive to negative. As T_0 increases further, quantum effects are destroyed and the classical limit will be reached so that $R \to 0$. As a result, for some intermediate value of T_0 the non-reciprocity will reach a maximum (negative) value. This is clearly seen in Fig. 2a where for $T_0 \approx 0.4$ the maximum rectification performance is achieved.

Furthermore, we see that, the rectification direction is controlled by the sign of the angular velocity Ω, thus allowing a greater flexibility to reconfigure "on the fly" the direction of the heat current. This can be understood from the equality $\frac{\mathcal{T}_{R_1R_3}}{\mathcal{T}_{R_2R_3}}[\omega,\Omega] = 1/(\frac{\mathcal{T}_{R_1R_3}}{\mathcal{T}_{R_2R_3}}[\omega,-\Omega])$ which is directly derived from Eq. (15) and Eq. (16). Specifically, due to this equality, in the frequency region where $|W(\omega_1,\omega_2,T_0)|$ is large (for a fixed average temperature T_0), the behavior of $\frac{\mathcal{T}_{R_1R_3}}{\mathcal{T}_{R_2R_3}}$ as a function of ω will turn from decreasing (increasing) function to increasing (decreasing) function when $\Omega \to -\Omega$. Thus the function K (defined in Eq. (19)) and correspondingly the rectification parameter R will change sign when we reverse the angular velocity Ω.

Finally, a 3D plot for the rectification R versus k_C and the angular velocity Ω is shown in Fig. 4. In these calculations the spring constant that couples the particles R_1, R_2, R_3 with the heat baths is taken to be $k = 1$. We see that the maximum rectification of $R_{max} = 1.6 \times 10^{-3}$ is observed for $k_C \approx 0.65$ and $\Omega \approx \pm 0.02$ near the origin. The non-monotonic behavior of R versus k_c is associated with an impedance mismatch between the two chains associated with the central junction lattice (with coupling constant k_c) and the one-dimensional chain of the bath (which involves coupling constants $k = 1$).

V. CONCLUSIONS

We have proposed the use of the Coriolis force in order to break time-reversal symmetry and induce thermal rectification in a ballistic three terminal nano-junction. Two of these terminals are attached to a hot and a cold reservoir, respectively, while the third one is attached to a probe reservoir whose temperature is self-consistently adjusted such that the net current towards this reservoir is zero. The nano-junction consists of a symmetric lattice which is placed on a rotating platform. Using non-equilibrium Green's function formalism we have calculated the rectification effect up to second-order in the temperature difference between the two reservoirs. We conclude that the Coriolis-induced rectification effect is of quantum mechanical nature and its direction and magnitude depend on Ω. It will be interesting to extend this study beyond the ballistic limit and investigate the effects of non-linearity and disorder. The latter phenomena can be important to any realistic structure where phonon-phonon interactions and structural imperfections are generally also present.

[1] S. Lepri, R. Livi, & A. Politi, Phys. Rep. **377**, 1 (2003).
[2] A. Dhar, Adv. Phys. **57**, 457 (2008).
[3] C. W. Chang, D. Okawa, H. Garcia, A. Majumdar, and A. Zettl, Phys. Rev. Lett, **101**, 075903 (2008).
[4] D. L. Nika, S. Ghosh, E. P. Pokatilov, and A. A. Balandin, Appl. Phys. Lett. **94**, 203103 (2009).
[5] N. Li, J. Ren, L. Wang, G. Zhang, P. Hänggi, and B. Li, Rev. Mod. Phys. **84**, 1045 (2012).
[6] G. Zhang & B. Li, NanoScale **2**, 1058 (2010).
[7] C. R. Otey, W. T. Lau, S. Fan, Phys. Rev. Lett. **104**, 154301 (2010); H. Iizuka, S. Fan, J. Appl. Phys. **112**, 024304 (2012).
[8] P. Ben-Abdallah, S-A. Biehs, Appl. Phys. Lett. **103**, 191907 (2013)
[9] E. Nefzaoui, J. Drevillon, Y. Ezzahri, K. Joulain, Appl. Opt. **53**, 3479 (2014); E. Nefzaoui, K. Joulain, J. Drevillon, Y. Ezzahri, Appl. Phys. Lett. **104** , 103905 (2014).
[10] L. Wang, B. Li, Phys. World **21**, 27 (2008); B. Li, L. Wang, G. Casati, Phys. Rev. Lett. **93**, 184301 (2004).
[11] B. Li, L. Wang, G. Casati, Appl. Phys. Lett. **88**, 143501 (2006).
[12] L. Wang, B. Li, Phys. Rev. Lett **99**, 177208 (2007); L. Wang, B. Li, Phys. Rev. Lett. **101**, 267203 (2008).
[13] L. Zhang, J-Sheng Wang, B. Li, Phys. Rev B **81**, 100301(R) (2010).
[14] Y. Ming, Z. X. Wang, Z. J. Ding, H. M. Li, N. J. Phys. **12**, 103041 (2010).
[15] E. Pereira, Phys. Lett. A **374**, 1933 (2010).
[16] Huanan Li and Tsampikos Kottos, Phys. Rev. E **91**, 020101(R) (2015).
[17] L. Landau and L. Lifshitz, *Statistical Physics*, 3rd ed. (Pergamon, New York, 1980).

[18] J.-S. Wang, B. K. Agarwalla, H. Li, and J. Thingna, Front. Phys. 9, 673 (2013).
[19] J. Schwinger, J. Math. Phys. **2**, 407 (1961); L. V. Keldysh, Sov. Phys. JETP **20**, 1018 (1965).
[20] H. Haug and A.-P. Jauho, *Quantum Kinetics in Transport and Optics of Semiconductors*, 2nd ed. (Springer, New York, 2008).
[21] R. J. Rubin and W. L. Greer, J. Math. Phys. **12**, 1686 (1971).